Chemosphere 307 (2022) 135863

Contents lists available at ScienceDirect

Chemosphere

journal homepage: www.elsevier.com/locate/chemosphere

Molecular dynamics simulation study of covalently bound hybrid coagulants (CBHyC): Molecular structure and coagulation mechanisms

Yuxia Liu [a], Shihan Cheng [b], Xueying Yang [c], An Xue [b], Zhenshan Li [b], Daniel S. Alessi [d], Kurt O. Konhauser [d], Huazhang Zhao, Dr [b,*]

[a] State Kety Laboratory of Petroleum Pollution Control, State Key Laboratory of Heavy Oil Processing, Department of Chemical Engineering and Environment, China University of Petroleum-Beijing, Beijing, 102249, China
[b] Key Laboratory of Water and Sediment Sciences (Ministry of Education), Department of Environmental Engineering, Peking University, Beijing, 100871, China
[c] State Key Laboratory of Petroleum Pollution Control, CNPC Research Institute of Safety and Environmental Technology, Beijing, 102206, China
[d] Department of Earth and Atmospheric Sciences, University of Alberta, Edmonton, Alberta, T6G 2E3, Canada

HIGHLIGHTS

- MD simulation was employed to elucidate the microstructure and dynamic process of CBHyC.
- CBHyC aggregates shaped with hydrophilic ammonium-Si-Al chains enclosing hydrophobic core.
- Strong electrostatic attractions and weak van der Waal forces were the driving forces.
- Driving forces between target contaminant and CBHyC affect the size and stability of aggregate.

GRAPHICAL ABSTRACT

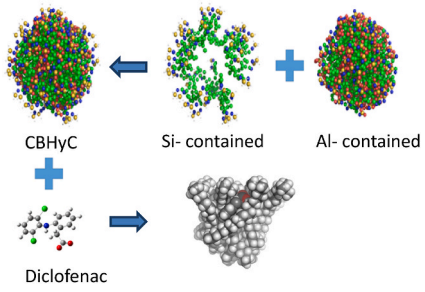

ARTICLE INFO

Handling Editor: Chang-Ping Yu

Keywords:
Coagulation
Organics
Hydrophobicity
Molecular dynamics simulation
Wastewater

ABSTRACT

Covalently-bound organic silicate-aluminum hybrid coagulants (CBHyC) have been shown to efficiently remove low molecular weight organic contaminants from wastewater. However, the interaction dynamics and motivations during the coagulation of contaminant molecules by CBHyC are limited. In this study, a molecular dynamics (MD) simulation showed that CBHyC forms core-shell structure with the aliphatic carbon chains gather inside as a core and the hydrophilic quaternary ammonium-Si-Al complexes disperse outside as a shell. This wrapped structure allowed the coagulant to diffuse into solutions easily and capture target contaminants. The adsorption of anionic organic contaminants (e.g., diclofenac) onto the CBHyC aggregates was driven equally by van der Waals forces and electrostatic interactions. Cationic organic contaminants (e.g., tetracycline) were seldom bound to CBHyC because of substantial repulsive forces between cationic molecules and CBHyC. Neutrally-charged organic molecules were generally bound through hydrophobic interactions. For adenine and thymine deoxynucleotide, representatives of antibiotic resistance genes, van der Waals forces and electrostatic interaction became the dominant driving force with further movement for adenine and thymine, respectively. Driving forces between target contaminant and coagulant directly affect the size and stability of formed aggregate, following the coagulation efficiency of wastewater treatment. The findings of this study enrich the database of aggregation

* Corresonding author. Tel.: +86 (010) 62758748; Fax: +86 (010) 62756526.
E-mail addresses: liuyuxia_mm@163.com (Y. Liu), xuean@iee.pku.edu.cn (A. Xue), zhaohuazhang@pku.edu.cn (H. Zhao).

https://doi.org/10.1016/j.chemosphere.2022.135863
Received 10 February 2022; Received in revised form 1 May 2022; Accepted 24 July 2022
Available online 9 August 2022

behavior between low molecular weight contaminants and CBHyC and contribute to further and efficient application of CBHyC in wastewater treatment.

1. Introduction

Coagulation is widely used in the removal of contaminants during wastewater treatment (Bratby, 2016). It is an attractive technology because of ease of operation, simple design, its cost-effectiveness and replacement upgradable (Wang et al., 2013). Organic and inorganic contaminants in wastewater can be destabilized and aggregated by coagulants through charge neutralization, adsorption and being incorporated or encompassed by a net coating (Stumm and Morgan, 1962; Stumm and O'Melia, 1968), and then separated from wastewater through settling. Conventional aluminum- or iron-based coagulants, and their polymers, are effective in removing turbidity, color and high molecular organic compounds (e.g., polymeric aromatic hydrocarbons and phenolic compounds like polyphenols) from wastewaters, including those associated with pulp and paper, dyeing, coking, landfill leachates (Zhao et al., 2008; Chang et al., 1999; Wei et al., 2009; Yang et al., 2010; Li et al., 2017a). However, emerging low molecular weight (anionic surfactants and their metabolites or coproducts, personal care products, and endocrine-disrupting compounds), hydrophilic and polar molecules (e.g., natural organic matter like fulvic acid, biocarbonate) in domestic sewage and drinking water plants are difficult to remove using conventional aluminum- or iron-based coagulants (Geng et al., 2018; Chen et al., 2015). Current coagulation technologies are hampered by their contaminant-specific removal ability and need to expand advanced wastewater treatment technologies to meet different water quality objectives, which will definitely increase treatment time and capital cost. Fortunately, a new class of material, covalently bound organic-silicate-aluminum hybrid coagulants (CBHyC), have shown great promise in the efficient removal of these challenging classes of organic contaminants (Geng et al., 2018; Boyer and Singer, 2008; Zhao et al., 2016a; Tan and Kilduff, 2007; Chu et al., 2018).

CBHyC is synthesized through polymerization reactions between the Si-hydroxyls in a silane coupling agent and the Al-hydroxyls in an Al-based coagulant by hydrolysis to form covalent Si–O–Al bonds (Fig. S1) (Zhao et al., 2009a, 2009b). Silane groups coupled with an octadecyl-ammonium group provided as the Si source, contain special organic groups (-R), alkoxyls (-OR') connected to the Si atom and cationic quaternary ammonium group which would lead to a linear structure in hybrid coagulants and enhance the coagulation efficiency (Zhao et al., 2009a, 2016a). These coagulants offer advantages of previous inorganic polymer coagulants, including ionic type (e.g., polyaluminum sulfate and poly-aluminum chloride) and complex coagulants (e.g., polymeric ferroaluminum chloride and polyaluminum silicate chloride) to remove color, turbidity, and high weight molecular contaminants (Zhao et al., 2016a; Mroczko and Zimoch, 2020; Hu et al., 2006; Tang et al., 2015; Chen et al., 2018). By controlling the Al concentration and choosing proper silicon source, the organic functional groups associated with CBHyC can be coupled to the inorganic component to improve the charge neutralization and increase its molecular weight for the rapid removal of the soluble low molecular weight contaminants (Zhao et al., 2009a, 2016a).

Coagulation performance is closely related to the structure of coagulant. Accordingly, knowledge of the factors affecting the structure of CBHyC has increased significantly (Zhao et al., 2008; Chang et al., 1999; Sharp et al., 2006; Shi et al., 2007). Meanwhile, it was speculated that CBHyC may interact with low molecular weight contaminants through charge neutralization, ion exchange, enmeshment and hydrophobic adsorption by experimental techniques. Since CBHyC has higher positive charge density, degree of polymerization, and molecular weight because of its special structure of inorganic components and organic components (long carbon chain quaternary ammonium groups positively charged) connected via covalent bonds. Yet to our knowledge, the microstructure of CBHyC and the underlying interaction dynamics and motivations during the coagulation of low molecular weight contaminant by CBHyC are limited. Such information is critical to optimizing the coagulation process and exploring the underlying factors affecting the coagulation efficiency, further developing more efficient coagulation process that can treat both wastewater and water to meet quality standards.

Molecular dynamics (MD) simulation, based on Newtonian mechanics by interatomic potentials or molecular mechanical force fields, is employed to study the structure and dynamics of macromolecules or aggregates during the motion of individual target molecules (Bermudez et al., 2016; Chen et al., 2019). MD simulation is able to solve problems without time and cost constraints because of lengthy experimental trials. With rapid increases in computational power (e.g., computational speed and parallelization of processes, data storage volume, graphics processing units) and expanded simulation methods, MD simulation can accurately mimic and elucidate the conformational, functional, and dynamic changes of biochemical processes and atom-atom interactions (Chen et al., 2019; Pall et al., 2020). MD simulations are extensively used in food processing, biological chemistry, material engineering and drug synthesis (Bermudez et al., 2016; Gupta et al., 2011; Moghaddasi et al., 2018). In recent two decades, MD and theoretical studies were widely employed to explore the correlation between structure and properties of materials and to investigate the general reaction characteristics and mechanisms, then the influencing factors from molecular level (Liu et al., 2018a, 2018b; Shao et al., 2020, 2021).

In this study, we employed MD simulations to investigate the microstructure of CBHyC under various silicon-aluminum ratios, as well the interaction dynamics and motivations of CBHyC with various small molecular organic compounds, including diclofenac (an organic anion), tonalide (neutrally charged), and tetracycline (an organic cation), as well as the nucleotides adenine and thymine which represent antibiotic resistance genes. These target contaminants were applied as personal care products and pharmaceutics and have been detected in water supplies and wastewater effluents around world (Chu et al., 2017, 2018; Chen et al., 2018). Meanwhile, these target contaminants are typically persistent and exhibit adverse ecological impacts and contribute to formation of disinfection by-products when adding common disinfectants (e.g., chlorine or ozone) (Chu et al., 2017). The results of this study provide a theoretical basis for optimization of coagulation processes of CBHyC and improvement of advanced wastewater treatment efficiency.

2. Simulating methodology

The optimization of molecular geometry and calculation of atomic electrostatic potential fit charges (ESP fit charges) were performed by Gaussian09 program with the level of HF/6-31G* (Car and Parrinello, 1985; Parr et al., 1989; Li et al., 2017b), followed by introducing Antechamber program to produce corresponding RESP potential with AMBER14ffSB force field (Wang et al., 2004). The software package GROMACS 2018 was used for all MD simulations (Van Der Spoel et al., 2005).

2.1. Structural simulation

CBHyC were synthesized by reacting aluminum chloride [$AlCl_3$] with 3-(trimethoxysilyl)propyl-n-octadecyldimethyl-ammonium chloride [$C_{18}H_{37}N(CH_3)_2\ C_3H_6Si(OCH_3)_3Cl$], synthesis procedures are summarized in Fig. S1. SOM, SOA, SAD and SAT were introduced, and SOM/SOA, SOM/SAD, and SOM/SAT systems (including 12 independent

Table 1
Description of basic units of MD simulating and reaction process during CBHyC synthesis.

Name	Formula	Molecular structure	Coarse grain model	Reaction
SOM	$RSi(OCH_3)$			
SOA	$RSi(OAl)_3$			SOM + $AlCl_3$→SOA
SAD	$RSi(OAl)_2$–Al–$Si(OAl)_2R$			SOA + NaOH→SAD
SAT	$RSi(OAl)_2$–Al– Si(OAl)R-Al-$Si(OAl)_2R$			SAD + NaOH→SAT

Note: 'R' represents residues on side chain ($C_{18}H_{37}N(CH_3)_2C_3H_6$). Red, grey, blue, white, cyan and pink correspond to oxygen, carbon, nitrogen, hydrogen, silicon and aluminum in molecular structure. Green, yellow, white, blue and red correspond to carbon chain ($(CH_2)_4$), organic silicon ($Si(CH_2)_2$), aluminum-oxygen (Al–O), nitrogen chain ($NCH_2(CH_3)_2C_2H_4$) and methoxy (OCH_3) in coarse grain model.

Table 2
Concentration of Si and Al under different SOM/SOA, SOM/SAD, and SOM/SAT simulating systems (Unit: M).

SOM/SOA system				SOM/SAD system				SOM/SAT system			
SOM	SOA	Si	Al	SOM	SAD	Si	Al	SOM	SAT	Si	Al
0.12	0	0.12	0	0.12	0	0.12	0	0.12	0	0.12	0
0.08	0.04	0.12	0.12	0.08	0.02	0.12	0.1	0.08	0.013	0.12	0.093
0.04	0.08	0.12	0.24	0.04	0.04	0.12	0.2	0.04	0.026	0.12	0.187
0	0.12	0.12	0.36	0	0.06	0.12	0.3	0	0.04	0.12	0.28

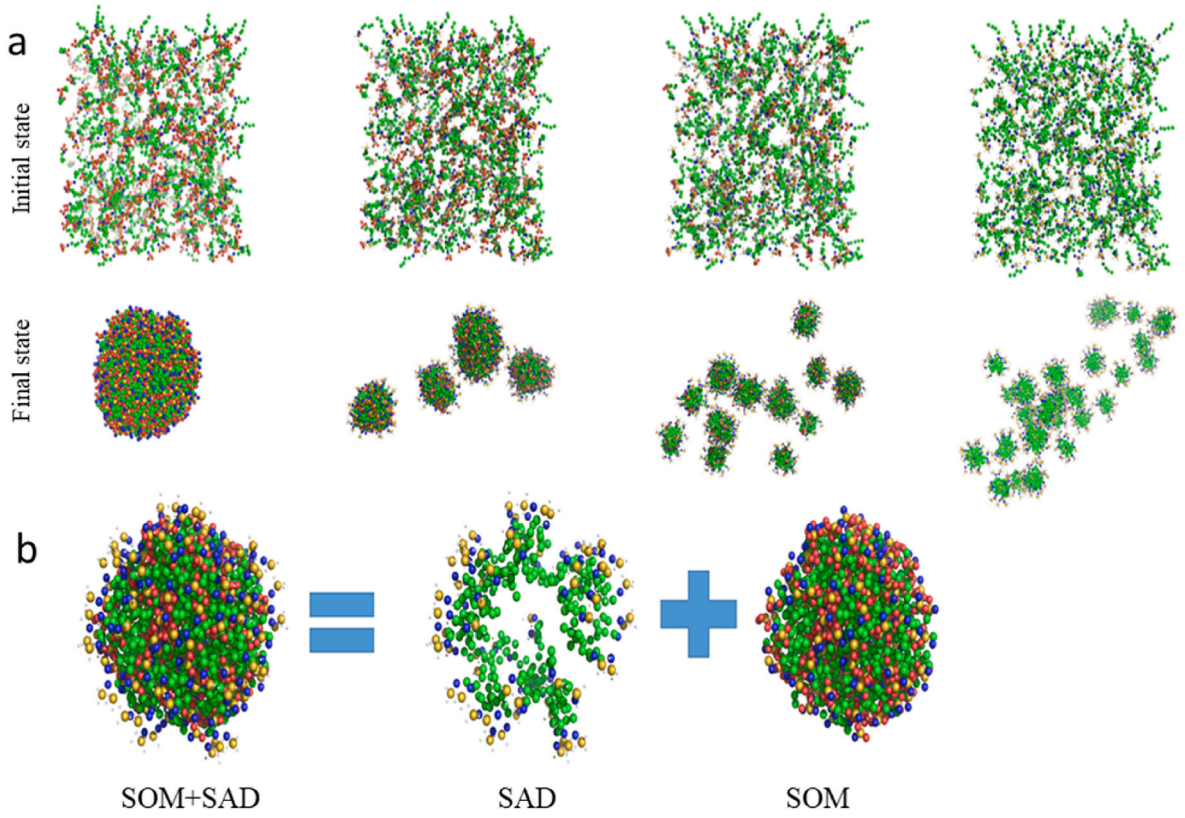

Fig. 1. (a) Initial and final state of CBHyC in SOM/SOA system, aggregates from left to right correspond to Si/Al ratios of 0.12:0, 0.12:0.12, 0.12:0.24, 0.12:0.36; (b) Microstructure of CBHyC simulated from SOM/SAD system (concentration of Si and Al were 0.12 and 0.1 M, respectively). Green corresponds to the hydrophobic carbon chain, yellow, white, blue and red correspond to Si, Al, N and O atoms, respectively. (For interpretation of the references to color in this figure legend, the reader is referred to the Web version of this article.)

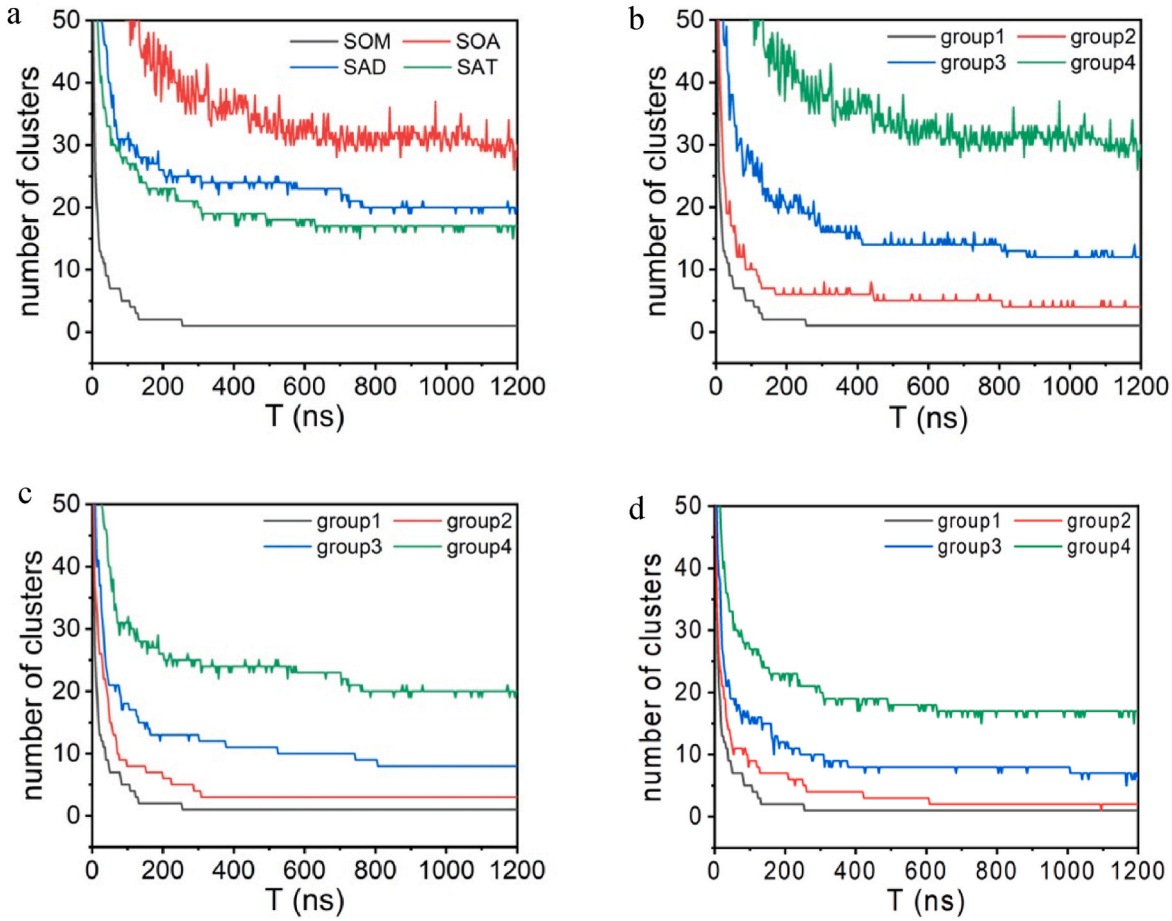

Fig. 2. Number of aggregates under different simulating systems: (a) Individual SOM, SOA, SAD and SAT condition; (b) SOM/SOA system; (c) SOM/SAD system; (d) SOM/SAT system.

runs) were performed to explore the spatial configuration of hybrid coagulant. Molecular configuration and coarse-grain geometry of SOM, SOA, SAD and SAT were shown in Table 1. It is noteworthy that SOA was resulted from reaction between SOM and $AlCl_3$, and SAD and SAT were formed under hydrolysis reactions of NaOH in SOA system. SAD and SAT were introduced to explore the effect of silicon structure on the formation of CBHyC coagulant. Various Si:Al ratios were reached by restrain the concentration of Si to 0.12 M and increase the concentration of Al from 0 to 0.12, 0.24, and 0.36 M gradually (Table 2). The initial configuration of hybrid coagulant cluster used in MD simulations was derived from a 20 × 20 × 20 nm orthorhombic solvent box. The topological parameters were set using the coarse-grain martini force field. A production MD was carried out under the temperature of 300 K for 1.2 μs.

2.2. Mechanistic exploration

Initially, CBHyC and target contaminant were solvated into a rectangular water box with the size of 7.3 × 7.3 × 7.3 nm^3 (containing 12,000 water molecules). TIP3P model was selected to simulate and stuff the solvent water (Jorgensen et al., 1983). 15 of Na^+ and 30 of Cl^- ions were added to neutralize the system, and the total ionic strength of simulated solvent was similar to that under lab condition. MD simulations were performed with AMBER14ffSB force field (Wang et al., 2004). The initial configuration of hybrid coagulant was simplified as a 4 × 4 × 1 array comprised of 16 quaternary ammonium cations, with nitrogen atoms fixed on the head of the quaternary ammonium cations. The distance between contaminant and nitrogen atom of CBHyC was 1.0 nm. The binding process of five target contaminants with CBHyC were investigated, including organic anions (diclofenac), neutrally charged organic molecule (tonalide), organic cations (tetracycline), and two representatives of antibiotic resistance genes, adenine and thymine deoxynucleotide. The initial configuration and molecular structure of CBHyC molecule and target contaminants were shown in Fig. S2. The Visual Molecular Dynamics (VMD) software was used for trajectory visualization and analysis (Humphrey et al., 1996).

1000 steps of energy minimization were conducted for the simulation system stuffed with solvent water, CBHyC molecule and specific target contaminants to eliminate potential atom collisions. After energy minimization, system was relaxed by the execution of a NPT (isothermal-isobaric statistical ensemble) (298 K, 1 bar) ensemble simulation for 0.5 ps (Mudi and Chakravarty, 2004; Lin et al., 2017). The Berendsen pressure coupling (Parrinello and Rahman, 1981) and the velocity rescaling thermostat (Bussi et al., 2007) were used for pressure and temperature coupling. Structures with lowest energy were chosen for the following MD simulation. The movement velocity of atoms was decided by Maxwell distribution randomly. Then the simulated hybrid coagulant molecules were frozen to produce similar configuration to that under experimental condition, and a production MD was performed for 30 ns. The production time of 30 ns was chosen because above which the parameters (e.g., bond angle between hydrogen bond donate and atom acceptor, COM distance between target contaminant center and quaternary ammonium groups associated with CBHyC, and neighbor water molecule number surrounded around any atom associated with target contaminant molecule) levelled off.

In the simulations, three-dimensional periodic boundary conditions

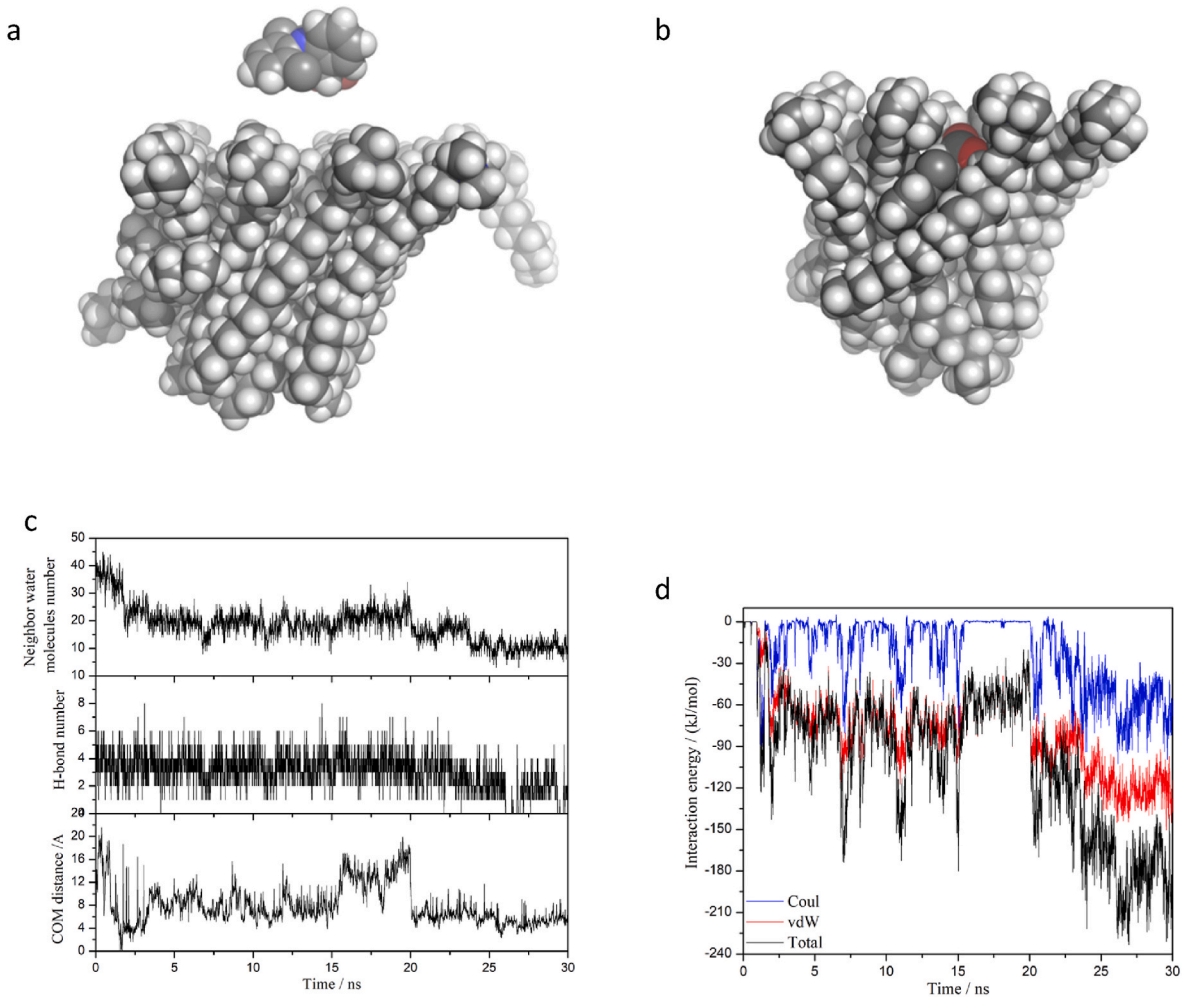

Fig. 3. (a) Initial state of diclofenac anions containing simulating system, blue ball corresponds to nitrogen atom, and red ball corresponds to oxygen atom; (b) Final state of diclofenac anions containing system; (c) Number of water molecules surrounded around diclofenac anions, the COM distance between diclofenac anions and CBHyC molecule, and number of hydrogen bond associated with diclofenac anions during the simulating coagulation process; (d) Interaction forces driving the adsorption of diclofenac anions onto CBHyC molecule. Black line corresponds to the total driving forces, red line corresponds to van der Waals forces, and blue line corresponds to electrostatic interactions. (For interpretation of the references to color in this figure legend, the reader is referred to the Web version of this article.)

were applied. The total simulation time was set to 1 fs, and the conformation was saved every 10 ps. The van der Waals interactions were truncated with a cutoff distance of 12 Å, while the electrostatic interactions were computed using Particle-mesh Ewald (PME) method (Darden et al., 1993). The PME algorithm was used to calculate long-range electrostatic interactions (Darden et al., 1993). The LINear Constraint Solver (LINCS) algorithm was used to maintain solute bonds at their equilibrium values (Hess et al., 1997), and the SETTLE (based on the Cartesian coordinate system, can be straightforwardly integrated into standard MD packages, which employ the SHAKE or RATTLE algorithm in their constraint routines, referred to as "SETTLE") algorithm was used to constrain bonding length of O–H and bonding angle of H–O–H (Miyamoto and Kollman, 1992).

3. Results

3.1. Microstructure of coagulant

To elucidate the microstructure of CBHyC, SOM/SOA, SOM/SAD, and SOM/SAT systems with various Si:Al ratio conditions (including 12 independent runs) were performed (Table 2). Within 1.2 μs of equilibrium time, hybrid coagulant molecules formed different types of aggregates (Fig. 1). Green ball showed extremely strong aggregation ability which represents the long carbon chain, and Al contained components were hydrophilic and tend to disperse into solutions in coarse-grain geometry. Interestingly, the final configurations of all three systems presented the following characteristics: (1) For SOM only system, absence of Al atom led to the formation of a single huge aggregate; (2) SOM aggregated to form a core inside, and SOA, SAD and SAT generally surrounded around the SOM aggregate to be a wrapped shell (Fig. S3); (3) The numbers of aggregates were similar under same Si and Al concentrations (Fig. 2). Above results indicate that CBHyC forms core-shell structure with the aliphatic carbon chains gather inside as a core by hydrophobic attraction and the positively charged hydrophilic quaternary ammonium-Si-Al complexes disperse outside by electrostatic repulsion. This wrapped structure allows it to be stable in storage, but also to remove contaminants through the synergistic effect of the core and shell components.

The spatial structure of CBHyC under various Si:Al ratios was explored, as shown in Fig. 2. The number of aggregations increased from left to right for 0, 0.12, 0.24, and 0.36 M of Al conditions. With the number of aggregations increased, the size of aggregates decreased substantially, indicating that the coagulant molecule was getting hard to assemble. In other words, the aggregation capability was negatively correlated with Al concentration in solution. Given that Al atoms in the system are abundant, then a simple extrapolation suggested that each

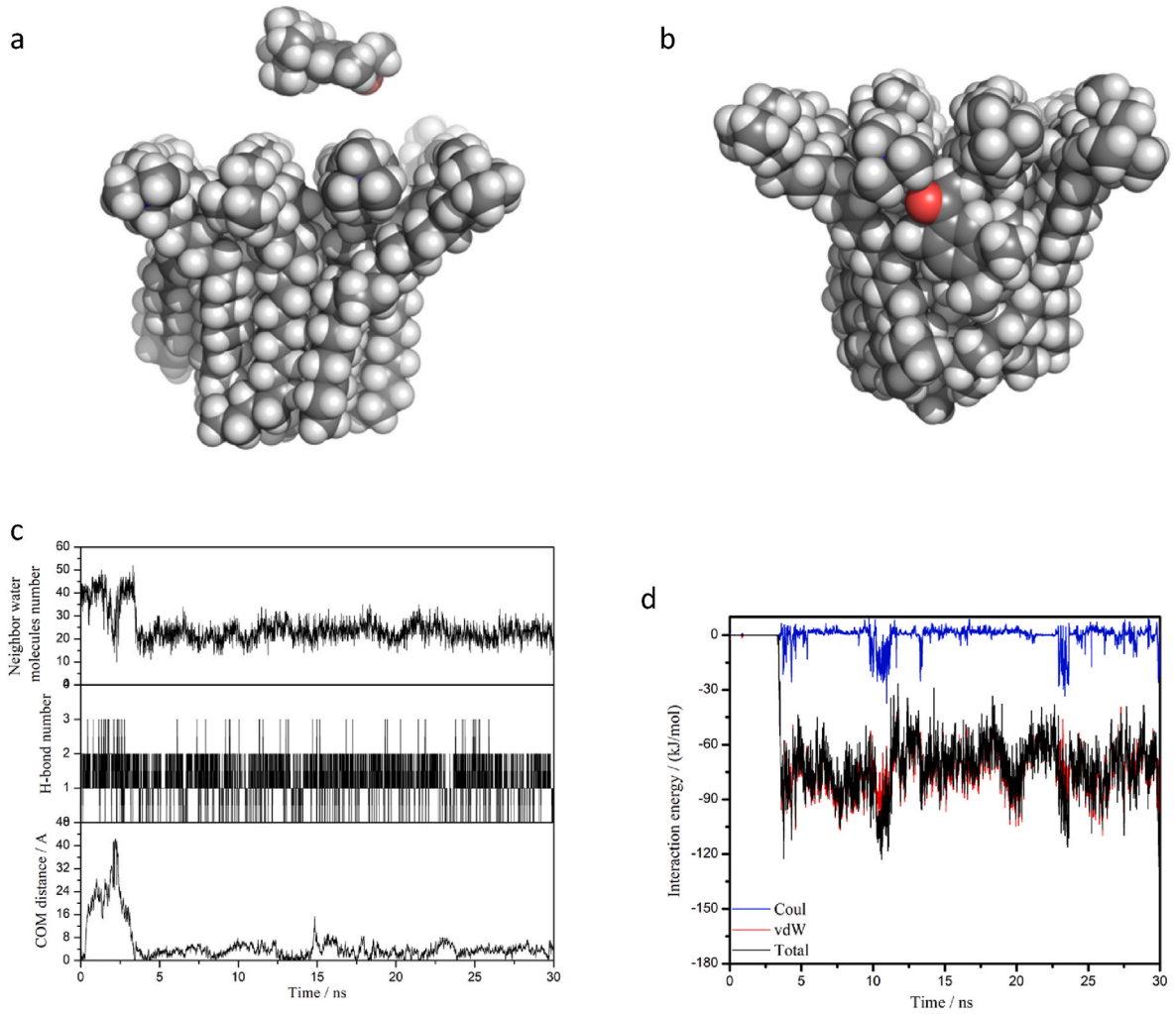

Fig. 4. (a) Initial state of tonalide molecule containing simulating system, red ball corresponds to oxygen atom; (b) Final state of tonalide molecule containing system; (c) Number of water molecules surrounded around tonalide molecule, the COM distance between tonalide molecule and CBHyC molecule, and number of hydrogen bond associated with tonalide molecule during the simulating coagulation process; (d) Interaction forces driving the adsorption of tonalide molecule onto CBHyC molecule. Black line corresponds to the total driving forces, red line corresponds to van der Waals forces, and blue line corresponds to electrostatic interactions. (For interpretation of the references to color in this figure legend, the reader is referred to the Web version of this article.)

coagulant molecule will form a tiny aggregate, and size of the tiny aggregate equals to the size of single coagulant molecule. Long carbon chain associated with SOM molecules was easy to assemble through van der Waals forces. By contrast, hydrophilic Al- atoms from SOA, SAD and SAT were easy to interact with water molecules and diffuse into solutions. For individual SOM, SOA, SAD and SAT system, the aggregation size follows the order of SOA > SAD > SAT > SOM (Fig. 2), and the aggregation capability follows the order of SOM > SAT > SAD > SOA.

3.2. Coagulation mechanism

3.2.1. Organic anions

Diclofenac was chosen as a representative of organic anions. As shown in Fig. 3, two benzene rings of diclofenac molecule were totally encapsulated into the head of CBHyC structure, with the oxygen atom tails still exposed outside (red ball in Fig. 3b). The COM distance between diclofenac and the upper surface of hybrid coagulant sharply decreased from ~20 Å to 6 Å and the number of water molecules around diclofenac molecules decreased from 40 to 20 during the first 5 ns of dispersive motion. Meanwhile, numbers of hydrogen bond around diclofenac molecules were stable, demonstrating a fast but weak adsorption of diclofenac onto CBHyC. It is noteworthy that accompanying with this adsorption process, water molecules were still existed in the interfacial region of diclofenac. As a result, the diclofenac molecules were easily to desorb from CBHyC. After 20 ns of dispersion motion, the COM distance decreased further to below 6 Å, and water molecules and hydrogen bond reduced slightly as well. The diclofenac molecules move towards to the side carbon chain in CBHyC, which is mainly driven by van der Waals interactions in addition to slight electrostatic interactions (Fig. 3d). From 23 ns on, diclofenac molecules diffused to nitrogen plane, the COM distance remained to ~6 Å, and water molecules and hydrogen bonds decreased further. The electrostatic interaction energy from positive nitrogen atoms and negative diclofenac ligands was ~60 kJ/mol, while the van der Waals force energy resulting from diclofenac captured by methyl groups increased from 60 kJ/mol to ~120 kJ/mol. This indicates that van der Waals forces and electrostatic interactions collectively drive the adsorption of diclofenac onto CBHyC, but van der Waals forces resulted from hydrophobic interactions dominated the coagulation process.

3.2.2. Neutrally charged organic molecules

Tonalide, a polycyclic musk widely used as fragrance additive in numerous consumer products, was used as a representative to model the dispersion motion of neutrally charged organic molecule during adsorption onto CBHyC. As shown in Fig. 4, tonalide attached to the carbon chain of CBHyC, and benzene ring parallel to the long carbon

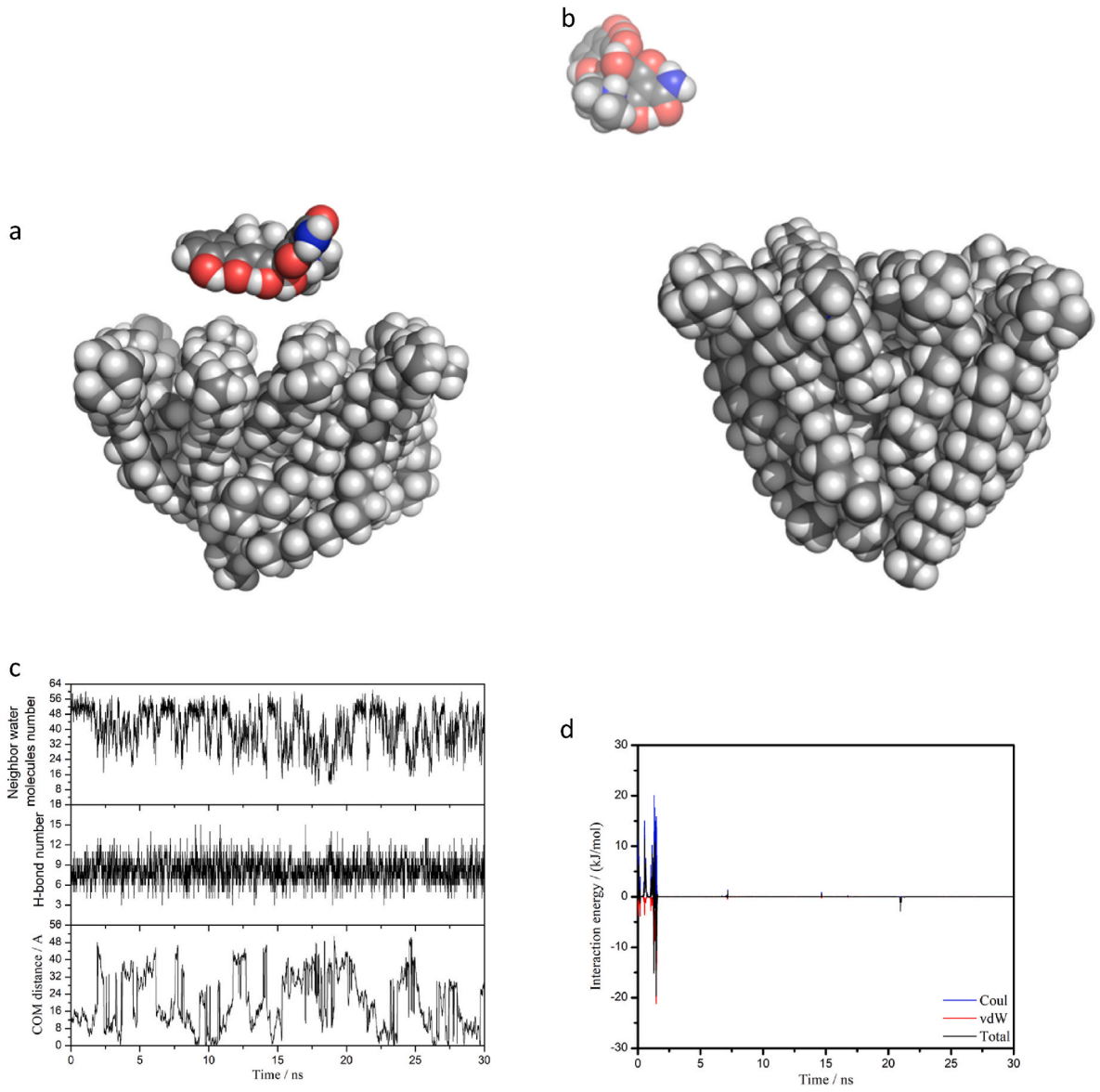

Fig. 5. (a) Initial state of tetracycline cation containing simulating system, blue ball corresponds to nitrogen atom, and red ball corresponds to oxygen atom; (b) Final state of tetracycline cation containing system; (c) Number of water molecules surrounded around tetracycline cation, the COM distance between tetracycline cation and CBHyC molecule, and number of hydrogen bond associated with tetracycline cation during the simulating coagulation process; (d) Interaction forces driving the adsorption of tetracycline cation onto CBHyC molecule. Black line corresponds to the total driving forces, red line corresponds to van der Waals forces, and blue line corresponds to electrostatic interactions. (For interpretation of the references to color in this figure legend, the reader is referred to the Web version of this article.)

chain. The number of water molecules surrounded around tonalide molecule decreased from 40 to 20, and remained constant to the end, suggesting a dehydration reaction. COM distance increased from ~4.5 Å to 42 Å in the first 3.5 ns of dispersion motion period, above which it decreased to ~3 Å sharply and then remained constant, which suggests that tonaline molecules adhere closely to the polar nitrogen surface. The number of hydrogen bond around tonalide molecule remained constant. Tonalide is neutrally charged and generates no electrons, thus there is no electrostatic attractions with positively charged CBHyC molecule. van der Waals forces remained constant to 75 kJ/mol, which is the major driving force of the adsorption process.

3.2.3. Organic cations

In this simulation system, tetracycline molecules always dispersed freely and did not show adsorption to the CBHyC molecule, which suggests that there is no interaction action between tetracycline and CBHyC molecule. As shown in Fig. 5, during the whole dispersion motion, the number of water molecules (12–60) around tetracycline molecules, the numbers of hydrogen bond (3–15) and the COM distance (0–50) exhibited a wide range of fluctuation. Potential interaction energy between tetracycline molecule and CBHyC levelled off at zero, though significant electrostatic repulsive interaction generated from positive tetracycline molecules and positive CBHyC adsorbents and van der Waals forces resulted from polar tetracycline and polar adsorbents dominated at the beginning. Finally, positively charged tetracycline molecule was repelled far away from positively charged CBHyC surface with no potential interaction energy.

3.2.4. Adenine and thymine deoxynucleotide

Adenine deoxynucleotide bound to the long carbon chain of CBHyC, and the five-atom ring associated with adenine deoxynucleotide molecule paralleled with the long carbon chain of a CBHyC molecule. As shown in Fig. 6, the number of water molecules around adenine molecule decreased from 43 to 16, and hydrogen bond decreased from 20 to

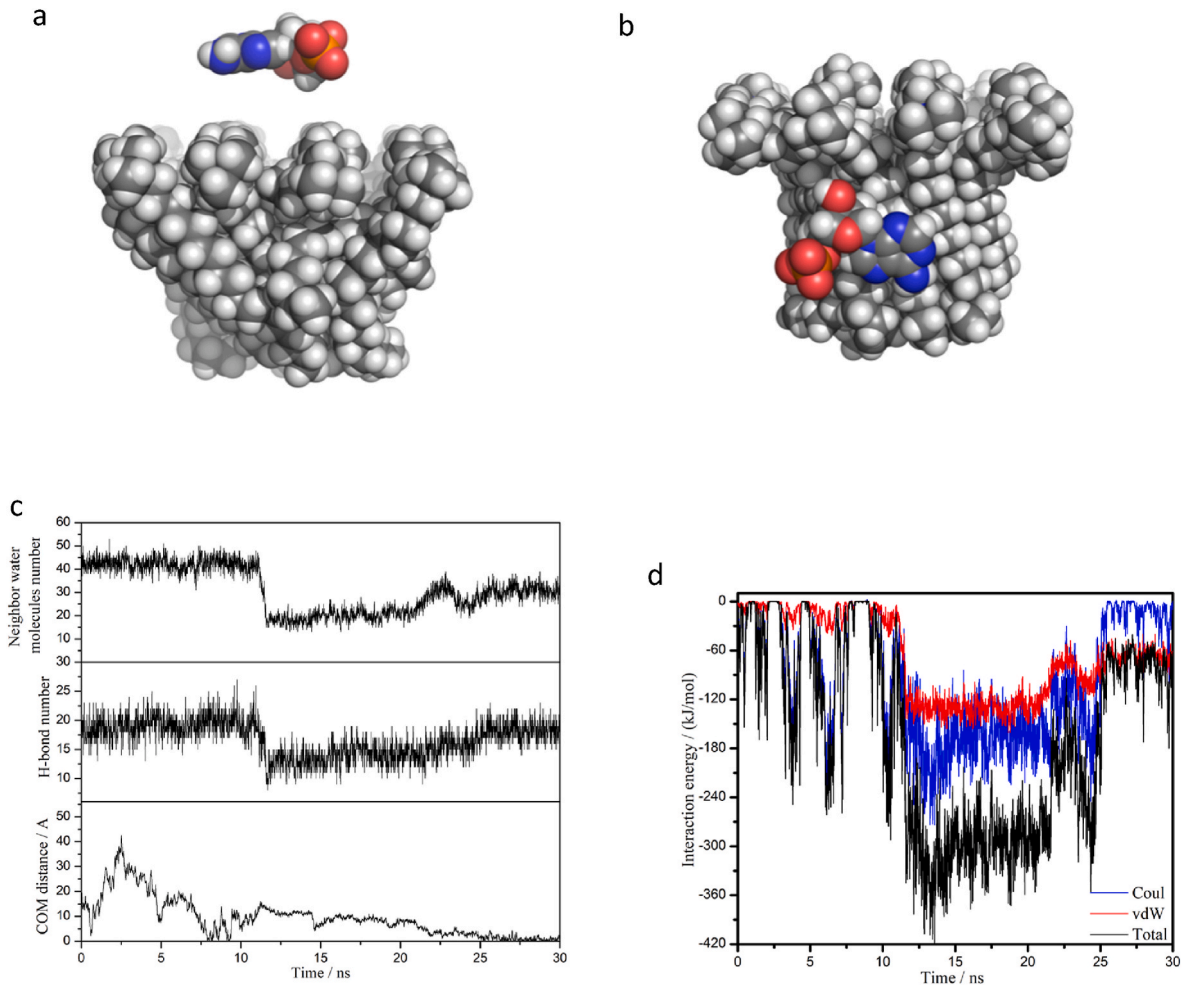

Fig. 6. (a) Initial state of adenine deoxyribonucleotide molecule containing simulating system, blue ball corresponds to nitrogen atom, and red ball corresponds to oxygen atom; (b) Final state of adenine deoxyribonucleotide molecule containing system; (c) Number of water molecules surrounded around adenine deoxyribonucleotide molecule, the COM distance between adenine deoxyribonucleotide molecule and CBHyC molecule, and number of hydrogen bond associated with adenine deoxyribonucleotide molecule during the simulating coagulation process; (d) Interaction forces driving the adsorption of adenine deoxyribonucleotide molecule onto CBHyC molecule. Black line corresponds to the total driving forces, red line corresponds to van der Waals forces, and blue line corresponds to electrostatic interactions. (For interpretation of the references to color in this figure legend, the reader is referred to the Web version of this article.)

11 during the first 12 ns of dispersive motion, suggesting the dewatering phenomena during the dispersion motion. After 12 ns of dispersive motion, water molecules and hydrogen bond increased slowly and then remained stable until 25 ns of dispersive motion. COM distance increased from 13 Å to 42 Å initially, and then decreased for a long decrease period until to 2 Å. During the first 25 ns of dispersion motion, the energy contribution from the electrostatic energy (increased from 0 to ~ 180 kJ/mol) is remarkably larger than that from van der Waals forces (increased from 0 to ~120 kJ/mol). The adenine molecules bound closely to the polar nitrogen surfaces of a CBHyC molecule and electrostatic interactions played a principal role. After 25 ns of dispersion motion, van der Waals forces energy decreased from 120 to 90 kJ/mol and contributed to the unique driving forces. During the process, adenine molecules tended to be adsorbed onto the carbon chain nearby, meanwhile the increase of the number of water molecules and hydrogen bonds strengthened the van der Waals forces.

The movement process of thymine deoxynucleotide molecule bound to CBHyC molecule was shown in Fig. 7. As shown in Fig. 7, the thymine molecules dispersed in the reaction cell during the first 7 ns of simulating process. From 7 to 17 ns of movement process, the number of water molecules around thymine decreased from 37 to 23, the number of hydrogen bond decreased to below 15, and the COM distance fluctuated within the range of 0–6 Å. After 17 ns, the number of water molecules and hydrogen bond increased gradually to the initial state, while the COM distance fluctuated within the range of 0–16 Å. Interaction forces driving the binding of thymine onto CBHyC molecule exhibited that the total binding energy was around 300 kJ/mol during the 7–17 ns of dispersion motion, and the van der Waals force contributed to around 120 kJ/mol, while the electrostatic interaction contributed to 180 kJ/mol. After 17 ns, the total binding energy decreased to around 180 kJ/mol, and the van der Waals forces and the electrostatic interactions decreased to around 60 kJ/mol and 120 kJ/mol, respectively. Electrostatic interactions were still the most driving forces. At the end of the simulation, van der Waals forces disappeared, and weak electrostatic interactions became the only driving forces, suggesting that desorption behavior of thymine from CBHyC molecule surface might happen.

4. Discussions

In this study, our simulation results suggested that CBHyC forms core-shell structure with the aliphatic carbon chains gather inside as a core and the hydrophilic quaternary ammonium-Si-Al complexes disperse outside as a shell. Under low pH conditions, CBHyC aggregated to form a core with organic silicon gathered inside, and organic Si–O–Al and Si–Al polymers generally surrounded around to be a wrapped shell which prevented the organic silicon from contacting with water

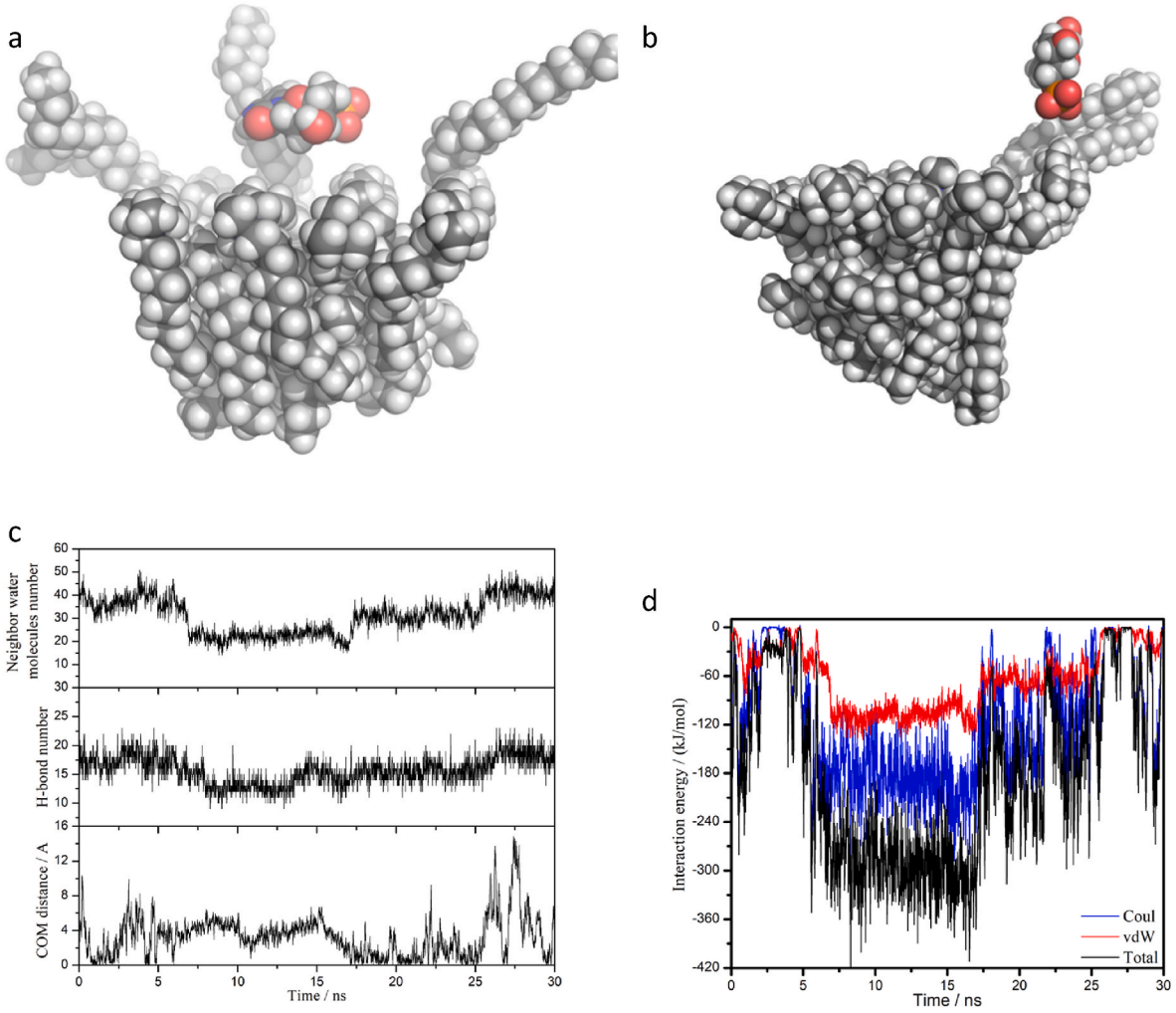

Fig. 7. (a) Initial state of thymine deoxyribonucleotide molecule containing simulating system, and red ball corresponds to oxygen atom; (b) Final state of thymine deoxyribonucleotide molecule containing system; (c) Number of water molecules surrounded around thymine deoxyribonucleotide molecule, the COM distance between thymine deoxyribonucleotide molecule and CBHyC molecule, and number of hydrogen bond associated with thymine deoxyribonucleotide molecule during the simulating coagulation process; (d) Interaction forces driving the adsorption of thymine deoxyribonucleotide molecule onto CBHyC molecule. Black line corresponds to the total driving forces, red line corresponds to van der Waals forces, and blue line corresponds to electrostatic interactions. (For interpretation of the references to color in this figure legend, the reader is referred to the Web version of this article.)

molecules. With increasing pH values, organic Si–Al polymers destabilized and get polymerized to form organic Si–O–Al. Since Al and Si are covalently bonded, Al does not readily hydrolyze nor does it undergo deprotonation of surface hydroxyl groups like a product derived by simply mixing inorganic and organic components, a compact and stable molecular structure is expected in CBHyC. The results in this study are consistent with microscopic images, which showed that CBHyC is submicron aggregates (100–900 nm of diameter) and reticular formation was observed on their edges (Zhao et al., 2016a). The cross-linked structure led to convex-concave porous structure which provided larger surface area and more adsorption sites, promoting charge neutralization, bridging performances and friction force acting among the flocs (Wang et al., 2020). With the decrease of Si/Al molar ratios, the aggregations get sparse and smaller, the chain-net structure became destroyed and the holes among the nets became much bigger (Wang et al., 2020), showing a low stability to form self-crosslinked silane coupling agents of reticular configuration (Zhao et al., 2016b). The Si–O–Al bond between Al and the silane agents hinders the self-crosslinking and produce relatively loose aggregates and coarse microstructure (Liu et al., 2018c). Consequently, with the increase of hydrophilic Al atoms in solution, coagulant molecule was easy to diffuse into solutions and getting hard to assemble.

Our molecular dynamics simulating results suggest that the interaction between CBHyC and dissolved contaminants with highly dehydration effects was mainly through electrostatic attractions; while for those contaminants without hydrophilic groups, CBHyC generally interacted with them mainly by weak van der Waals forces resulting from hydrophobic interactions. Wrapped Si–O–Al shell hydrolyzed and enmeshed particles and colloids from solutions, while hydrophobic SOM core of CBHyC coagulants captured contaminants by electrostatic and hydrophobic interactions. Coagulation mechanisms for different contaminants were summarized in Table 3. The electrostatic interactions between anions and CBHyC were confirmed in simulating dispersion motion of anionic diclofenac, adenine and thymine deoxynucleotide, which electrostatic forces played a primary role in the aggregation process. For diclofenac, a representative of anionic small organic molecule, diclofenac molecules were close to either the N atoms or the carbon chains of CBHyC coagulants, suggesting that van der Waals forces enhanced by both the H-bond from a carboxyl group and the hydrophobic forces from two benzene rings rather than charge neutralization alone mainly drive the aggregation process. For base adenine and thymine, hydrogen bond allowed them to form stable basic pairs, since DNA molecules generally existed as double helixes. Meanwhile, ademine was prevented from adsorption onto nitrogen surface of

Table 3
Comparison of coagulation mechanism for different pollutants.

Pollutant	Diclofenac	Tonalide	Tetracycline	Adenine	Thymine
Charge	−1	0	1	−2	−2
Electrostatic forces (%)	0.33	0	/	0.6–0	0.6–0.67
van der Waals forces (%)	0.67	1	/	0.4–1	0.4–0.33
Binding energy (kJ/mol)	180	75	/	330–90	300–120
Binding strength	Stable, strong	Stable, strong	No binding	Strong to weak	Strong to weak to zero
Water molecules	40-22-16-13	40–20	irregular	43-16-30	37-23-30-37
COM distance	8-12-6	4	irregular	0	4
Hydrogen bond	4–2	3	irregular	20-12-18	18-12-15-18
Binding site	Nitrogen surface	Carbon chain	/	Nitrogen surface-carbon chain	Nitrogen surface

CBHyC because of dual-ring structure and the disappearance of electrostatic interaction. As a result, weak van der Waals forces became the dominant forces for adsorption. While, thymine deoxynucleotide molecule was close to nitrogen surface and no more van der Waals forces existed. Consequently, electrostatic interaction and hydrogen bond between the thymine deoxynucleotide molecule carboxyl or hydroxyl and the CBHyC nitrogen atoms became the main driving forces in thymine removal. By contrast, electroneutral organic tonalide molecules was easily adsorbed though hydrophobic forces between benzene ring and the long carbon chain.

Our in silico simulating results provided fundamental mechanisms for those experimental studies, which showed that CBHyC can interact with anionic surfactants, low molecular weight and high soluble organic contaminants. Collectively, these organic contaminants include highly unsaturated and phenolic compounds and aliphatic compounds with atomic ratio of $0.3 < O/C < 0.8$ and $1.0 < H/C < 2.0$ regions. Sulfur-containing compounds with higher O/C are also the potential target for CBHyC, which may contain hydrophilic acidic functional groups (carboxyl or sulfonic acid groups), hydrophobic benzene rings and long carbon chains, and usually have higher water solubility due to their hydrophilic functional groups and low molecular weight (Geng et al., 2018; Chu et al., 2018; Chen et al., 2018). The interaction between CBHyC and organic contaminants involve electrostatic attraction and ion-exchange reactions facilitated by covalently bound quaternary ammonium group which was independent of pH contribute to the coagulation (Geng et al., 2018; Zhao et al., 2016a). Chu et al. (2018) indicated that both electrostatic attraction and hydrophobic interaction were responsible for the removal of organophosphates by CBHyC, and the removal efficiency was more than 98%. In this case, contaminants bind through electrostatic attractions are relatively strong, while contaminants bind through van der Waals forces are easy to be desorbed and thus decrease the removal efficiency. In other words, the driving forces and patterns of target contaminant bound to CBHyC are dependent on the structure of the target contaminant by influencing the binding sites of CBHyC molecule. Since CBHyC has large molecular weight, contaminants carried by CBHyC were easy to settle from the water phase to the solid phase. Previous studies indicated that CBHyC exhibited different coagulation behavior due to the fact that various Si:Al ratios, Si sources and polymerized techniques can generates different zeta potentials, Al species distribution, and organic functional groups (Zhao et al., 2009a, 2009b; Zimoch and Mroczko, 2020). Zeta potential of CBHyC is derived from the synergic effect including the amount of quaternary ammonium groups and positive charges on hydroxyl-aluminum (Zhao et al., 2009a, 2009b). In addition, particle size and dosage of coagulants have been proven to be important parameters influencing the hydrolysis rates and aggregation formations (Sun et al., 2019; Yu et al., 2021). Experimental determination of these parameters for various emerging contaminants might be direct, but such practices are constrained by time and energy cost and complex to operate.

Compared to other treatment methods, coagulation is easy to operate and cost-effectiveness. Conventional coagulation is widely used as either a single process or pretreatment process for microfiltration/ultrafiltration to remove turbidity, color, particles, colloids and high molecular weight organic macromolecules. However, conventional coagulation is constrained to remove low molecular weight organic contaminants, hydrophilic and polar molecules. Coagulation with CBHyC provides possibilities to overcome limitations of conventional coagulation, since covalent Si–O–Al bonds shell destabilizes and hydrolyses into flocs and enmeshes particles and colloids, and a linear structure connected with cationic quaternary ammonium groups captures dissolved molecules by electrostatic and hydrophobic interactions.

5. Conclusions

Molecular dynamic simulation was employed to explore the microstructure of CBHyC under various silicon-aluminum ratios, as well the interaction dynamics and motivations of CBHyC with various organic compounds. It was found that CBHyC is submicron aggregates, with hydrophobic carbon chain gathered as a core and is surrounded and protected by hydrophilic Al-contained components. With the decrease of Si/Al molar ratios, the chain-net structure became destroyed and the aggregations get sparse and smaller, indicating that the coagulant molecule was getting hard to assemble. The interaction between CBHyC and dissolved contaminants with highly dehydration effects was mainly through electrostatic attractions; while for those contaminants without hydrophilic groups, CBHyC generally interacted with them mainly by weak van der Waals forces resulting from hydrophobic interactions. Accordingly, calculating and exploring the chemical reactions and binding energy during coagulation between CBHyC and target contaminants may also be interesting to attempt. An expanded study will involve designing tailored hybrid coagulant structures with proper hydrophobic/hydrophilic component to remove target contaminants for wastewater treatment.

Author contributions

Yuxia Liu (First author): Conceptualization, Formal analysis, Funding acquisition, Writing. **Shihan Cheng**: Data curation, Formal analysis, Methodology, Visualization. **Xueying Yang**: Formal analysis. **An Xue** (Corresponding author): Methodology, Visualization, Software. **Zhenshan Li**: Validation. **Daniel S. Alessi**: Editing, Validation. **Kurt O. Konhauser**: Editing, Validation. **Huazhang Zhao** (Corresponding author): Conceptualization, Funding acquisition, Supervisor, Editing.

Declaration of competing interest

The authors declare that they have no known competing financial interests or personal relationships that could have appeared to influence the work reported in this paper.

Acknowledgement

This work was supported by the National Science Fund for Distinguished Young Scholars (Grant No. 21925801), the National Natural Science Fund of China (Grant No. 42007336 and 21878002), the National Key Research and Development Program of China (2016YFC0402505), the Fundamental Research Funds for the Central Universities (ZX20210084) and the Open Project Program of State Key

Laboratory of Petroleum Pollution Control (PPC2020004), CNPC Research Institute of Safety and Environmental Technology.

Appendix A. Supplementary data

Supplementary data to this article can be found online at https://doi.org/10.1016/j.chemosphere.2022.135863.

References

Bermudez, M., Mortier, J., Rakers, C., Sydow, D., Wolber, G., 2016. More than a look into a crystal ball: protein structure elucidation guided by molecular dynamics simulations. Drug Discov. Today 21 (11), 1799–1805. https://doi.org/10.1016/j.drudis.2016.07.001.

Boyer, T.H., Singer, P.C., 2008. Stoichiometry of removal of natural organic matter by ion exchange. Environ. Sci. Technol. 42 (2), 608–613. https://doi.org/10.1021/es071940n.

Bratby, J., 2016. Coagulation and Flocculation in Water and Wastewater Treatment, third ed. ed., vol. 15. IWA Publishing, London, pp. 507–510.

Bussi, G., Donadio, D., Parrinello, M., 2007. Canonical sampling through velocity rescaling. J. Chem. Phys. 126 (1), 7. https://doi.org/10.1063/1.2408420.

Car, R., Parrinello, M., 1985. Unified approach for molecular dynamics and density functional theory. Phys. Rev. Lett. 55 (22), 2471–2474. https://doi.org/10.1103/PhysRevLett.55.2471.

Chang, E.E., Chiang, P.C., Chao, S.H., Liang, C.H., 1999. Effects of polydiallyldimethyl ammonium chloride coagulant on formation of chlorinated by products in drinking water. Chemosphere 39 (8), 1333–1346. https://doi.org/10.1016/S0045-6535(99)00036-3.

Chen, W., Zheng, H., Zhai, J., Wang, Y., Xue, W., Tang, X., Zhang, Z., Sun, Y., 2015. Characterization and coagulation–flocculation performance of a composite coagulant: poly-ferric-aluminum-silicate-sulfate. Desalination Water Treat. 56 (7), 1776–1786. https://doi.org/10.1080/19443994.2014.958109.

Chen, S., Yuan, Z.W., Hanigan, D., Westerhoff, P., Zhao, H.Z., Ni, J.R., 2018. Coagulation behaviors of new covalently bound hybrid coagulants (CBHyC) in surface water treatment. Separ. Purif. Technol. 192, 322–328. https://doi.org/10.1016/j.seppur.2017.10.036.

Chen, G., Huang, K., Miao, M., Feng, B., Campanella, O.H., 2019. Molecular dynamics simulation for mechanism elucidation of food processing and safety: state of the art. Compr. Rev. Food Sci. Food Saf. 18 (1), 243–263. https://doi.org/10.1111/1541-4337.12406.

Chu, K.H., Al-Hamadani, Y.A.J., Park, C.M., Lee, G., Jang, M., Jang, A., Her, N., Son, A., Yoon, Y., 2017. Ultrasonic treatment of endocrine disrupting compounds, pharmaceuticals, and personal care products in water: a review. Chem. Eng. J. 327 (1), 629–647. https://doi.org/10.1016/j.cej.2017.06.137.

Chu, Y.B., Li, M., Liu, J.W., Xu, W., Cheng, S.H., Zhao, H.Z., 2018. Molecular insights into the mechanism and the efficiency-structure relationship of phosphorus removal by coagulation. Water Res. 147, 195–203. https://doi.org/10.1016/j.watres.2018.10.006.

Darden, T., York, D., Pedersen, L., 1993. Particle mesh Ewald: an $N{\cdot}\log(N)$ method for Ewald sums in large systems. J. Phys. Chem. 98 (12), 10089–10092. https://doi.org/10.1063/1.464397.

Geng, C.X., Cao, N., Xu, W., He, C., Yuan, Z.W., Liu, J.W., Shi, Q., Xu, C.M., Liu, S.T., Zhao, H.Z., 2018. Molecular characterization of organics removed by a covalently bound inorganic-organic hybrid coagulant for advanced treatment of municipal sewage. Environ. Sci. Technol. 52 (21), 12642–12648. https://doi.org/10.1021/acs.est.8b03306.

Gupta, J., Nunes, C., Vyas, S., Jonnalagadda, S., 2011. Prediction of solubility parameters and miscibility of pharmaceutical compounds by molecular dynamics simulations. J. Phys. Chem. B 115 (9), 2014–2023. https://doi.org/10.1021/jp108540n.

Hess, B., Bekker, H., H.J.C.B., Fraaije, J.G.E.M. LINCS, 1997. A linear constraint solver for molecular simulations. J. Comput. Chem. 18 (12), 1463–1472. https://doi.org/10.1002/(SICI)1096-987X, 18:12199709.

Hu, C., Liu, H., Qu, J., Wang, D., Ru, J., 2006. Coagulation behavior of aluminum salts in eutrophic water: significance of Al13 species and pH control. Environ. Sci. Technol. 40 (1), 325–331. https://doi.org/10.1016/j.cis.2015.09.002.

Humphrey, W., Dalke, A., Schulten, K., 1996. VMD: visual molecular dynamics. J. Mol. Graph. 14 (1), 33–38. https://doi.org/10.1016/0263-7855(96)00018-5.

Jorgensen, W.L., Chandrasekhar, J., Madura, J.D., 1983. Comparison of simple potential functions for simulating liquid water. J. Chem. Phys. 79, 926. https://doi.org/10.1063/1.445869.

Li, J., Liu, X., Cheng, F., 2017a. Bio-refractory organics removal and floc characteristics of poly-silicic-cation coagulants in tertiary-treatment of coking wastewater. Chem. Eng. J. 324, 10–18. https://doi.org/10.1016/j.cej.2017.04.142.

Li, Y., Yang, Z., Wang, Y., Bai, Z., Zheng, T., Dai, X., Liu, S., Gui, D., Liu, W., Chen, M., 2017b. A mesoporous cationic thorium-organic framework that rapidly traps anionic persistent organic pollutants. Nat. Commun. 8 (1), 1354. https://doi.org/10.1038/s41467-017-01208-w.

Lin, Y.Q., Pan, D.Y., Li, J.M., Zhang, L.X., Shao, X.M., 2017. Application of Berendsen barostat in dissipative particle dynamics for nonequilibrium dynamic simulation. J. Chem. Phys. 146 (12), 124108 https://doi.org/10.1063/1.4978807.

Liu, Y., Liu, Z., Zeng, G., Chen, M., Jiang, Y., Shao, B., Li, Z., Liu, Y., 2018a. Effect of surfactants on the interaction of phenol with laccase: molecular docking and molecular dynamics simulation studies. J. Hazard Mater. 357, 10–18. https://doi.org/10.1016/j.jhazmat. 2018.05.042.

Liu, Z., Liu, Y., Zeng, G., Shao, B., Chen, M., Li, Z., Jiang, Y., Liu, Y., Zhang, Y., Zhong, H., 2018b. Application of molecular docking for the degradation of organic pollutants in the environmental remediation: a review. Chemosphere 203, 139–150. https://doi.org/10.1016/j. chemosphere.2018.03.179.

Liu, J.W., Cheng, S.H., Cao, N., Geng, C.X., He, C., Shi, Q., Xu, C.M., Ni, J.R., DuChanois, R.M., Elimelech, M., Zhao, H.Z., 2018c. Actinia-like multifunctional nanocoagulant for single-step removal of water contaminants. Nat. Nanotechnol. 14 (1), 64–71. https://doi.org/10.1038/s41565-018-0307-8.

Miyamoto, S., Kollman, P.A., 1992. Settle: an analytical version of the SHAKE and RATTLE algorithm for rigid water models. J. Comput. Chem. 13 (8), 952–962. https://doi.org/10.1002/jcc.540130805.

Moghaddasi, F., Housaindokht, M.R., Darroudi, M., Bozorgmehr, M.R., Sadeghi, A., 2018. Soybean oil-based nanoemulsion systems in absence and presence of curcumin: molecular dynamics simulation approach. J. Mol. Liq. 264, 242–252. https://doi.org/10.1016/j.molliq.2018.05.066.

Mroczko, D., Zimoch, I., 2020. Effectiveness of coagulation, sorption, and ion exchange processes in reduction of selected priority substances from surface waters. Desalination Water Treat. 199, 212–219. https://doi.org/10.5004/dwt.2020.26027.

Mudi, A., Chakravarty, C., 2004. Effect of the Berendsen thermostat on the dynamical properties of water. Mol. Phys. 102 (7), 681–685. https://doi.org/10.1080/00268970410001698937.

Pall, S., Zhmurov, A., Bauer, P., Abraham, M., Lundborg, M., Gray, A., Hess, B., Lindahl, E., 2020. Heterogeneous parallelization and acceleration of molecular dynamics simulations in GROMACS. J. Chem. Phys. 153 (13), 134110 https://doi.org/10.1063/5.0018516.

Parr, R.G., Gadre, S.R., Bartolotti, L.J., 1989. Density-functional theory of atoms and molecules. In: Horizons of Quantum Chemistry, vol. 76. Springer, Dordrecht, pp. 2522–2526.

Parrinello, M., Rahman, A., 1981. Polymorphic transitions in single crystals: a new molecular dynamics method. J. Appl. Phys. 52 (12), 7182–7190. https://doi.org/10.1063/1.328693.

Shao, B., Wang, J., Liu, Z., Zeng, G., Tang, L., Liang, Q., He, Q., Wu, T., Liu, Y., Yuan, X., 2020. $Ti_3C_2T_x$ MXene decorated black phosphorus nanosheets with improved visible-light photocatalytic activity: experimental and theoretical studies. J. Mater. Chem. 8 (10), 5171–5185. https://doi.org/10.1039/C9TA13610J.

Shao, B., Liu, Z., Zeng, G., Liu, Y., Liang, Q., He, Q., Wu, T., Pan, Y., Huang, J., Peng, Z., Luo, S., Liang, C., Liu, X., Tong, S., Liang, J., 2021. Synthesis of 2D/2D CoAl-LDHs/$Ti_3C_2T_x$ Schottky-junction with enhanced interfacial charge transfer and visible-light photocatalytic performance. Appl. Catal. B Environ. 286, 119867 https://doi.org/10.1016/j.apcatb.2020. 119867.

Sharp, E.L., Jarvis, P., Parsons, S.A., Jefferson, B., 2006. The impact of zeta potential on the physical properties of ferric−NOM flocs. Environ. Sci. Technol. 40 (12), 3934–3940. https://doi.org/10.1021/es051919r.

Shi, B., Wei, Q., Wang, D., Zhu, Z., Tang, H., 2007. Coagulation of humic acid: the performance of preformed and non-preformed Al species. Colloids and Surfaces A: Physicochem. Eng. Aspect. 296 (1), 141–148. https://doi.org/10.1016/j.colsurfa.2006.09. 037.

Stumm, W., Morgan, J.J., 1962. Chemical aspects of coagulation. J. - Am. Water Works Assoc. 54 (8), 971–994. https://doi.org/10.1002/j.1551-8833.1962.tb00922.x.

Stumm, W., O'Melia, C.R., 1968. Stoichiometry of coagulation. J. - Am. Water Works Assoc. 60 (5), 514–539. https://doi.org/10.1002/j.1551-8833.1968.tb03579.x.

Sun, H.Y., Jiao, R.Y., Xu, H., An, G.Y., Wang, D.S., 2019. The influence of particle size and concentration combined with pH on coagulation mechanisms. J. Environ. Sci. 82, 39–46. https://doi.org/10.1016/j.jes.2019.02.021.

Tan, Y., Kilduff, J.E., 2007. Factors affecting selectivity during dissolved organic matter removal by anion-exchange resins. Water Res. 41 (18), 4211–4221. https://doi.org/10.1016/j.watres.2007.05.050.

Tang, H., Xiao, F., Wang, D., 2015. Speciation, stability, and coagulation mechanisms of hydroxyl aluminum clusters formed by PACl and alum: a critical review. Adv. Colloid Interface Sci. 226, 78–85. https://doi.org/10.1016/j.cis.2015.09.002.

Van Der Spoel, D., Lindahl, E., Hess, B., Groenhof, G., Mark, A.E., Berendsen, H.J., 2005. GROMACS: fast, flexible, and free. J. Comput. Chem. 26 (16), 1701–1718. https://doi.org/10.1002/jcc.20291.

Wang, J., Wolf, R.M., Caldwell, J.W., Kollman, P.A., Case, D.A., 2004. Development and testing of a general amber force field. J. Comput. Chem. 25 (9), 1157–1174. https://doi.org/10.1002/jcc.20035.

Wang, J.P., Yuan, S.J., Wang, Y., Yu, H.Q., 2013. Synthesis, characterization and application of a novel starch-based flocculant with high flocculation and dewatering properties. Water Res. 47, 2643–2648. https://doi.org/10.1016/j.watres.2013.01.050.

Wang, S., Li, E., Li, J., Du, Z., Cheng, F., 2020. Preparation and coagulation-flocculation performance of covalently bound organic hybrid coagulant with excellent stability. Colloids and Surfaces A: Physicochem. Eng. Aspect. 600, 124966 https://doi.org/10.1016/j. colsurfa.2020.124966.

Wei, J., Gao, B., Yue, Q., Wang, Y., 2009. Effect of dosing method on color removal performance and flocculation dynamics of polyferric-organic polymer dual-coagulant in synthetic dyeing solution. Chem. Eng. J. 151 (1), 176–182. https://doi.org/10.1016/j. cej.2009.02.012.

Yang, Z.L., Gao, B.Y., Yue, Q.Y., Wang, Y., 2010. Effect of pH on the coagulation performance of Al-based coagulants and residual aluminum speciation during the treatment of humic acid–kaolin synthetic water. J. Hazard Mater. 178 (1), 596–603. https://doi.org/10.1016/j.jhazmat.2010.01.127.

Yu, K.F., Li, P., Li, H., Zhang, B., Yang, J., Huang, F.Y., Li, R., He, Y.L., 2021. Potential of coagulation to remove particle-associated and free-living antibiotic resistome from

wastewater. J. Hazard Mater. 406, 124295 https://doi.org/10.1016/j.jhazmat.2020.124295.
Zhao, H., Hu, C.Z., Liu, H.J., Zhao, X., Qu, J.H., 2008. Role of aluminum speciation in the removal of disinfection byproduct precursors by a coagulation process. Environ. Sci. Technol. 42 (15), 5752–5758. https://doi.org/10.1021/es8006035.
Zhao, H.Z., Peng, J.X., Lin, S., Zhang, Y., 2009a. Covalently bound organic silicate aluminum hybrid coagulants: preparation, characterization, and coagulation behavior. Environ. Sci. Technol. 43 (6), 2041–2046. https://doi.org/10.1021/es802965v.
Zhao, H.Z., Peng, J.X., Xue, A., Ni, J.R., 2009b. Distribution and transformation of Al species in organic silicate aluminum hybrid coagulants. Compos. Sci. Technol. 69 (10), 1629–1634. https://doi.org/10.1016/j.compscitech.2009.03.013.
Zhao, H.Z., Wang, L., Hanigan, D., Westerhoff, P., Ni, J.R., 2016a. Novel ion-exchange coagulants remove more low molecular weight organics than traditional coagulants. Environ. Sci. Technol. 50 (7), 3897–3904. https://doi.org/10.1021/acs.est.6b00635.
Zhao, H.Z., Wang, L., Chang, Y.Y., Xu, Y., 2016b. High-efficiency removal of perfluorooctanoic acid from water by covalently bound hybrid coagulants (CBHyC) bearing a hydrophobic quaternary ammonium group. Separ. Purif. Technol. 158, 9–15. https://doi.org/10.1016/j.seppur.2015.11.044.
Zimoch, I., Mroczko, D., 2020. The use of zeta potential measurement as a control tool of surface water coagulation. J. Ecol. Eng. 21 (3), 237–242. https://doi.org/10.12911/22998993/118273.